

# 1 **Advances in the development of a time-domain unstructured finite element** 2 **method for the analysis of waves and floating structures interaction**

3 Borja Serván-Camas and Julio García

4 Centre Internacional de Metodes Numerics en Enginyeria, C/ Gran Capitan s/n, Edificio C1,  
5 Campus Nord, UPC, 08034 Barcelona, Spain.

## 6 **Abstract**

7 Being capable of predicting wave-structure interaction in the time domain is of great interest for the  
8 offshore industry. However most computer programs used in the industry work in the frequency  
9 domain. Therefore, the main objective of this work is the development a time domain solver based  
10 on the finite element method capable of solving wave-structure interaction problems using  
11 unstructured meshes. We found good agreement between the numerical results we obtained and  
12 analytical solutions as well as numerical solutions obtained by other numerical method.

13  
14 **Keywords:** wave structure interaction; finite element; time domain; unstructured mesh.

## 15 **1. Introduction**

16 Wave structure interaction is a topic of great interest in naval and offshore engineering. This  
17 interest is growing in the last years due to the boost given by the development of the marine  
18 renewable energy field. In this context, the development of time-domain wave structure interaction  
19 programs is a main request from the industry.

20 Up to date the numerical simulation of wave structure interaction has been mostly carried  
21 out using the frequency domain. The reason might be that the computational cost of time domain  
22 simulations were too high and computational time was too large. Moreover, assumptions like linear  
23 waves and the harmonic nature of water waves made the frequency domain to be the right choice.  
24 However, nowadays computing capabilities make possible to carry out numerical simulations in the  
25 time domain in a reasonable time, with the advantage of making easier the coupling with other  
26 phenomena.

27 Regarding the numerical method usually adopted, the boundary element method (BEM) has  
28 dominated over others like finite element method (FEM). The main advantage of BEM over FEM  
29 resides in the fact that only boundary meshes are required, while FEM demands meshing the whole  
30 volume, with the corresponding increase in the number of variables of the discrete problem.  
31 However, despite of the higher number of variables required by FEM, it is not clear that BEM has  
32 to be more efficient. Mostly due to the sparse pattern in FEM and the large availability of iterative  
33 solver preconditioners that can improve the resolution of the corresponding linear system of  
34 equations. In [1] Cai et al. a heuristic comparison between both methods is given and demonstrate  
35 that a solution to the boundary value problem can be obtained more efficiently by the FEM.

36 In the last decade, there have been extensive applications of the finite element method  
37 (FEM) to free surface problems. For example, Oñate and García [2] presented a stabilized FEM for  
38 fluid structure interaction in the presence of free surface where the latter was modelled by solving a  
39 fictitious elastic problem on the moving mesh. In [3,4] Löhner et al. developed a FEM capable of  
40 tracking violent free surface flows interacting with objects. Also García et al. [5] developed a new  
41 technique to track complex free surface shapes. However, many works like the previous ones are  
42 based on solving the Navier-Stokes equations, too expensive computationally speaking when it  
43 comes to simulating many real problems regarding ocean waves interacting with floating structures,  
44 which can be more cheaply simulated using potential flow theory along with Stokes perturbation  
45 approximation.

46 Despite of the great effort invested in the last years to the development of FEM algorithms,  
47 to the authors' knowledge, yet there has not been developed a FEM for solving first order waves,  
48 based on Stokes perturbation, interacting with structures in the time domain using unstructured  
49 meshes. The use of structure or semi-structures meshes is a big limitation since it limits the

50 complexity of the geometry to be used. In this study we present a FEM for wave-structure  
 51 interaction that can be used with unstructured meshes. Besides, since it is based on Stokes wave  
 52 theory, no re-meshing or moving mesh technique are needed, which keeps computational costs and  
 53 times low. The algorithm has been adapted to include non-linear external forces, like those used to  
 54 define mooring systems, and variations on the pressure over the free surface.

## 55 2. Problem statement

### 56 2.1 Governing equations

57 We consider the first order diffraction-radiation problem of a floating body.

$$58 \nabla^2 \varphi = 0 \quad \text{in } \Omega \quad (1)$$

$$59 \partial_t \varphi + g\eta = -P_a / \rho + C \quad \text{in } z = 0 \quad (\text{dynamic free surface boundary condition}) \quad (2)$$

$$60 \partial_t \eta - \partial_z \varphi = 0 \quad \text{in } z = 0 \quad (\text{kinematic free surface boundary condition}) \quad (3)$$

$$61 \partial_z \varphi = 0 \quad \text{in } z = -H \quad (4)$$

$$62 \nabla \varphi \cdot \mathbf{n}_B = \mathbf{v}_B \cdot \mathbf{n}_B \quad \text{in } \Gamma_B \quad (5)$$

63 where  $\varphi$  and  $\eta$  are the first order potential and free surface elevation respectively;  $\Omega$  is the fluid  
 64 domain bounded by  $z = 0$ ;  $P_a$  is the atmospheric pressure;  $\rho$  is the water density;  $C$  is a constant  
 65 value;  $\Gamma_B$  represents the wetted surface of a floating body; and  $H$  is the water depth. The domain is  
 66 assumed to be infinite in the horizontal directions.

67

### 68 2.2 Velocity potential decomposition

69 The aim of this work is to simulate the dynamics of a floating body subjected to the action  
 70 of waves. To do so, we will first model the environment as the sum of a number of airy waves. This  
 71 can be expressed in terms of a velocity potential given by:

$$72 \psi = \sum_m \frac{A_m g}{\omega_m} \frac{\cosh(|\mathbf{k}_m|(H+z))}{\cosh(|\mathbf{k}_m|H)} \cos(|\mathbf{k}_m|(x \cos \alpha_m + y \sin \alpha_m - \omega_m t + \delta_m)) \quad (6)$$

73 where  $A_m$  are the wave amplitudes;  $\omega_m$  are the wave frequencies;  $\mathbf{k}_m$  are the wave numbers;  $\alpha_m$   
 74 are the wave directions; and  $\delta_m$  are wave phases. From this point on, we will refer to  $\psi$  as the  
 75 incident potential. This potential, along with the dispersion relation  $\omega_m^2 = g|\mathbf{k}_m| \tanh(|\mathbf{k}_m|H)$ , fulfils  
 76 Eqs. (1)-(4), and therefore is solution of the mathematical model in the absence of bodies.

77

78 Let  $\varphi = \psi + \phi$  be the solution to the governing equations. The equations to be fulfilled by  $\phi$  are

$$79 \nabla^2 \phi = 0 \quad \text{in } \Omega \quad (7)$$

$$80 \partial_t \phi + g\eta = -P_a / \rho + C' \quad \text{in } z = 0 \quad (\text{dynamic free surface boundary condition}) \quad (8)$$

$$81 \partial_t \eta - \partial_z \phi = 0 \quad \text{in } z = 0 \quad (\text{kinematic free surface boundary condition}) \quad (9)$$

$$82 \partial_z \phi = 0 \quad \text{in } z = -H \quad (10)$$

$$83 \nabla \phi \cdot \mathbf{n}_B = (\mathbf{v}_B - \nabla \psi) \cdot \mathbf{n}_B \quad \text{in } \Gamma_B \quad (11)$$

84

### 85 2.3 Radiation condition and wave absorption

86 We will make use of a Sommerfeld radiation condition at the edge of the computational  
 87 domain:

88  $\partial_t \phi + c \nabla \phi \cdot \mathbf{n}_R = 0$  in the surface limiting of the domain in the horizontal directions, and  $c$  is a  
 89 prescribed wave velocity. Wave dissipation is also introduced into the dynamic free surface  
 90 boundary condition by varying the pressure such that  $P_a / \rho = P_0 + \kappa(\mathbf{x}) \partial_z \phi$  where  $\kappa(\mathbf{x})$  is a  
 91 damping coefficient. Combining the dynamic and kinematic boundary condition, introducing the  
 92 wave absorption and choosing  $C' = P_0$ , the governing equations for  $\phi$  becomes:

$$93 \quad \nabla^2 \phi = 0 \quad \text{in } \Omega \quad (12)$$

$$94 \quad \partial_{tt} \phi = -g \partial_z \phi - \kappa(\mathbf{x}) \partial_t \partial_z \phi \quad \text{in } z = 0 \quad (13)$$

$$95 \quad \partial_z \phi = 0 \quad \text{in } z = -H \quad (14)$$

$$96 \quad \nabla \phi \cdot \mathbf{n}_B = (\mathbf{v}_B - \nabla \psi) \cdot \mathbf{n}_B \quad \text{in } \Gamma_B \quad (15)$$

$$97 \quad \partial_t \phi + c \nabla \phi \cdot \mathbf{n}_R = 0 \quad \text{in } \Gamma_R \quad (16)$$

$$98 \quad \eta = -\frac{1}{g} \partial_t \phi - \frac{P_a}{\rho g} + \frac{C'}{g} \quad \text{in } z = 0 \quad (\text{kinematic free surface boundary condition}) \quad (17)$$

### 99 3. Finite element formulation

100 The discrete variational problem:

$$101 \quad \int_{\Omega} \nabla v_h \cdot \nabla \phi_h d\Omega = \int_{\Gamma^B} v_h \cdot \widehat{\phi}_n^B d\Gamma + \int_{\Gamma^R} v_h \cdot \widehat{\phi}_n^R d\Gamma + \int_{\Gamma^{Z_0}} v_h \cdot \widehat{\phi}_n^{Z_0} d\Gamma + \int_{\Gamma^{Z-H}} v_h \cdot \widehat{\phi}_n^{Z-H} d\Gamma \quad \forall v_h \in Q_h \quad (18)$$

102 where  $\widehat{\phi}_n^B$ ,  $\widehat{\phi}_n^R$ ,  $\widehat{\phi}_n^{Z_0}$  and  $\widehat{\phi}_n^{Z-H}$  are the potential normal gradients corresponding to the Neumann  
103 boundary conditions on body, radiation boundary, free surface and bottom, respectively. The  
104 associated matrix form is:

$$105 \quad \overline{\overline{\mathbf{L}}}\phi = \mathbf{b}^B + \mathbf{b}^R + \mathbf{b}^{Z_0} + \mathbf{b}^{Z-H} \quad (19)$$

106

#### 107 3.1 Boundary conditions

108 The right hand side of Eq. (19) is implemented as follows:

$$109 \quad (\mathbf{b}^{Z_0})^{n+1} = -\overline{\overline{\mathbf{M}}}_{\Gamma^{Z_0}} \left( \frac{12}{g \Delta t^2 + 6\kappa(\mathbf{x}) \Delta t} (\phi^{n+1} - 2\phi^n + \phi^{n-1}) + \frac{10g \Delta t}{g \Delta t + 6\kappa(\mathbf{x})} (\phi_z^{Z_0})^n + \left( \frac{g \Delta t - 6\kappa(\mathbf{x})}{g \Delta t + 6\kappa(\mathbf{x})} \right) (\phi_z^{Z_0})^{n-1} \right)$$

110 (20)

111

$$112 \quad (\mathbf{b}^R)^{n+1} = \overline{\overline{\mathbf{M}}}_{\Gamma^R} (\phi_n^R)^{n+1} = \frac{1}{\Delta t} \overline{\overline{\mathbf{M}}}_{\Gamma^R} (\phi^n - \phi^{n-1}) \quad (21)$$

113

$$114 \quad (\mathbf{b}^B)^{n+1} = \overline{\overline{\mathbf{M}}}_{\Gamma^B} (\phi_n^B)^{n+1} \quad (22)$$

115

116 The free surface and pressure are computed by the following fourth order finite difference scheme:

$$117 \quad \eta^{n+1} = -\frac{1}{g \Delta t} \left( \frac{25}{12} \varphi^{n+1} - 4\varphi^n + 3\varphi^{n-1} - \frac{4}{3} \varphi^{n-2} + \frac{1}{4} \varphi^{n-3} \right) \quad (23)$$

$$118 \quad P^{n+1} = -\rho g z - \frac{\rho}{\Delta t} \left( \frac{25}{12} \varphi^{n+1} - 4\varphi^n + 3\varphi^{n-1} - \frac{4}{3} \varphi^{n-2} + \frac{1}{4} \varphi^{n-3} \right) \quad (24)$$

119

#### 120 3.2 Body dynamics

121 Integrating the pressure over the body surface, the resulting forces and moments are  
122 obtained. On the other hand, the body dynamics is given by the equation of motion:

$$123 \quad \overline{\overline{\mathbf{M}}}\mathbf{X}_{tt} + \overline{\overline{\mathbf{K}}}\mathbf{X} = \mathbf{F} \quad (25)$$

124 where  $\overline{\overline{\mathbf{M}}}$  is the mass matrix;  $\overline{\overline{\mathbf{K}}}$  is the hydrostatic restoring coefficient matrix;  $\mathbf{F}$  is the  
125 hydrodynamic forces induced over the body plus any other external forces; and  $\mathbf{X}$  represent the  
126 movement of the six degrees of freedom. we use a implicit Newmark's average acceleration method  
127 to carry out the temporal integration of Eq. (25)

128

#### 129 3.3 Free surface boundary condition for OWC calculations

130 In order to be able to simulate OWC devices, a non-linear free surface boundary condition  
 131 has been developed based on the characteristic curves of the Wells-turbines type used in these  
 132 devices. For instance, based on the manufacturer information and working in ideal conditions, the  
 133 Wavegen 18.5Kw turbine get a power output and pressure that relates to the flux as:

$$134 \quad p(q) = 0.0779|q|^3 - 0.065q^2 + 0.1933|q| \quad (26)$$

$$135 \quad P(q) = 164.07 \cdot q \cdot |q| \quad (27)$$

136 where p is the output power in kilowatts, P is the pressure drop across the turbine in Pascals, and q  
 137 is the instantaneous air flux flowing through the turbine in cubic meters per second. The pressure  
 138 obtained by eq. (27) is introduced into the dynamic condition of the free surface as

$$139 \quad \frac{\phi^{n+1} - 2\phi^n + \phi^{n-1}}{\Delta t^2} = -\frac{1}{12}g(\partial_z\phi^{n+1} + 10\partial_z\phi^n + \partial_z\phi^{n-1}) - \frac{1}{12\rho}(\partial_t P^{n+1} + 10\partial_t P^n + \partial_t P^{n-1}) \quad (28)$$

$$140 \quad \partial_t P^{n+1} \square (3P^{n+1} - 4P^n + P^{n-1}) / (2\Delta t) \quad (29)$$

## 141 4. Numerical results

### 142 4.1 Waves refracted by a vertical circular cylinder

143 In this section we solve the problem of a monochromatic wave interacting with a fix bottom  
 144 mounted circular cylinder. The analytical solution for the incident and scattered wave potential are  
 145 four in [6]. Next we compare numerical results obtained by the analytical solution with numerical  
 146 results obtained by our FEM schemes for the specific case of  $R = 1$ ,  $H = 1$ ,  $A = 0.1$ ,  $L = 2$ . Using  
 147  $g = 9.81$  and by mean of the dispersion relation for first order waves, we obtain the frequency value

148  $\omega = \sqrt{g\pi \tanh(\pi)} = 5.5411 \text{ rad/s}$ , and the wave period  $T = 1.1339 \text{ s}$ . Figure 1: Left: **Contour lines of**

149 **free surface elevation at  $t = nT$ . Comparison between analytical (solid line) and FEM (dot**

150 **line) results. Center: Pressure induced on the cylinder by the velocity potential at time  $t = nT$ .**

151 **Comparison between analytical (up) and FEM (down) results. Right: Horizontal force induced**

152 **over the cylinder. Comparison between analytical (solid line) and FEM (dots) results** left

153 compares the contour lines of the free surface elevation at any time  $t = nT$ . It can be observed that

154 the FEM solution mostly lie over the analytical solution. . Figure 1: Left: **Contour lines of free**

155 **surface elevation at  $t = nT$ . Comparison between analytical (solid line) and FEM (dot line)**

156 **results. Center: Pressure induced on the cylinder by the velocity potential at time  $t = nT$ .**

157 **Comparison between analytical (up) and FEM (down) results. Right: Horizontal force induced**

158 **over the cylinder. Comparison between analytical (solid line) and FEM (dots) results** center

159 compares the pressure distribution over the cylinder obtained by the analytical solution and the

160 FEM solution. Both pressure distributions are obtained using the same colour scale, with a

161 maximum value of 1500 and a minimum of 2000. Figure 1: Left: **Contour lines of free surface**

162 **elevation at  $t = nT$ . Comparison between analytical (solid line) and FEM (dot line) results.**

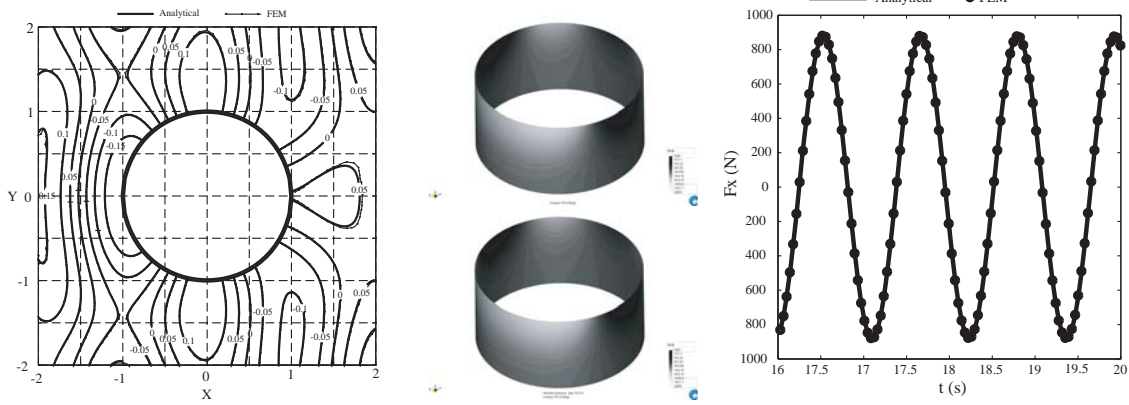
163 **Center: Pressure induced on the cylinder by the velocity potential at time  $t = nT$ . Comparison**

164 **between analytical (up) and FEM (down) results. Right: Horizontal force induced over the**

165 **cylinder. Comparison between analytical (solid line) and FEM (dots) results** right compares the

166 force induced over the cylinder obtained by the analytical solution and FEM. It can be seen that the

167 forces obtained in both ways are quite close to each other.

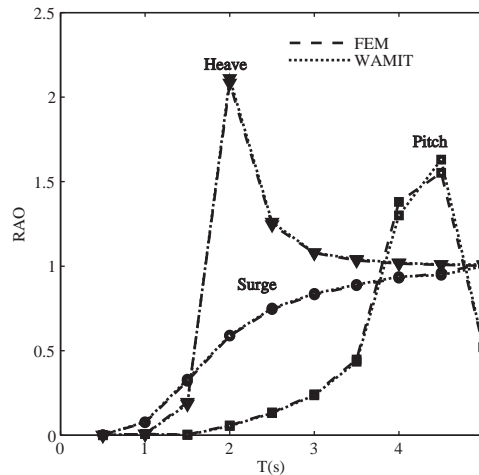


168  
169  
170  
171  
172  
173  
174  
175  
176  
177  
178  
179  
180  
181  
182  
183

**Figure 1:** Left: Contour lines of free surface elevation at  $t = nT$ . Comparison between analytical (solid line) and FEM (dot line) results. Center: Pressure induced on the cylinder by the velocity potential at time  $t = nT$ . Comparison between analytical (up) and FEM (down) results. Right: Horizontal force induced over the cylinder. Comparison between analytical (solid line) and FEM (dots) results

### 4.3 Freely floating circular cylinder

In this section we analyze the seakeeping behaviour of a freely floating cylinder subject to the action of monochromatic waves. The cylinder parameters are; Radius=1m; draft=0.5m;  $x_g=0$ ;  $y_g=0$ ;  $z_g=0$ ;  $I_{xx}/\text{Mass}=1$ ;  $I_{yy}/\text{Mass}=1$ ;  $I_{zz}/\text{Mass}=1$ . Simulations were carried out for periods ranging between half a second and five seconds. Figure 2 Response amplitude operator for freely floating cylinder. Circles (surge); triangles (heave); squares (pitch). compares the response amplitude operators (RAOs) obtained by the present FEM model and RAOs obtained by the well known program WAMIT, which is based on the BEM. Both results agree well and only some small differences are observed in the resonance area for the pitch movement, probably due to the different numerical dissipation added in that case in the BEM and FEM formulations.



184  
185  
186

**Figure 2** Response amplitude operator for freely floating cylinder. Circles (surge); triangles (heave); squares (pitch).

### 4.4 Oscillating water column test

187  
188  
189  
190  
191  
192  
193  
194  
195  
196

In this section, the FEM model was used to analyze the performance of an OWC device to absorb energy from waves. The OWC consist of a circular bell of 5 meters in diameter (inner), 0.5 meters in thickness, and 2.5 meter in draft. The water depth is 20 meters and the OWC device will be subject to the action of monochromatic waves with periods ranging between 3 and 5 seconds. The free surface elevation was analyzed within the chamber in the absence of the turbine ( $P=0$ ). Figure 3: **Response amplitude operator for oscillating water column.** shows response amplitude operators obtained as  $\xi = Q_{\max} / (A\pi R^2 \omega)$ , where  $Q_{\max}$  is the instantaneous flux amplitude;  $A$  is the wave amplitude;  $R$  is the inner radius of the OWC device;  $\omega$  is the wave frequency; and  $\xi$  represents the average amplitude of the free surface elevation within the device. Figure 3:

197 **Response amplitude operator for oscillating water column.** shows the RAOs under different  
 198 wave periods.

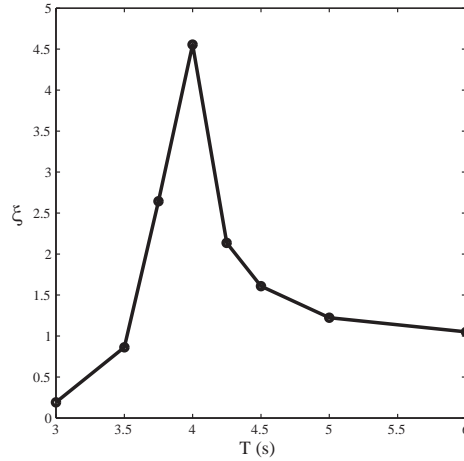


Figure 3: Response amplitude operator for oscillating water column.

200  
 201  
 202 The performance of the same OWC device was also analyzed after installing a Wells-type  
 203 turbine, the Wavegen 18.5Kw model. The imposition of Eq. (26) implies that the problem is no  
 204 linear anymore. Therefore, the performance of the system was analyzed for three wave amplitudes  
 205 and a range of periods. Table 1: **Oscillating water column results** summarizes the results obtained  
 206 from the simulation, where the columns named power provide the average power supplied by the  
 207 device, and the efficiency is obtained from dividing the average power by the power transported by  
 208 a wave front of 5 meters.  
 209

T(s)	A=0.1m		A=0.5m		A=1m	
	Power (kw)	Efficiency	Power (kw)	Efficiency	Power (kw)	Efficiency
3	0,079	13,38%	0,379	2,58%	0,923	1,57%
3.5	0,150	21,85%	0,762	4,44%	1,936	2,82%
4	0,203	25,87%	1,189	6,06%	3,135	3,99%
4.5	0,234	26,44%	1,587	7,17%	4,310	4,87%
5	0,254	25,65%	2,002	8,09%	5,590	5,64%
6	0,259	21,00%	2,654	8,62%	7,790	6,32%
7	0,242	15,97%	3,082	8,14%	9,483	6,26%

Table 1: Oscillating water column results

210  
 211 **5. Conclusions**

212 A FEM solver for wave structure interaction in the time domain has been presented. The  
 213 wave modelling is based on Stokes perturbation theory, which allows keeping the same  
 214 computational domain along the simulation. The FEM has been developed so unstructured meshes  
 215 can be used, no matter the complexity of the structure.

216 Both, the free surface and outlet boundary conditions are based on implicit schemes. They  
 217 have been introduced within the system matrix so that no iterations are required within the time step  
 218 to reach convergence among the Laplace and boundary conditions.

219 FEM results have been compared to analytical results available for a circular vertical  
 220 cylinder. The agreement between both solutions shows that the algorithms develop in this work  
 221 perform well. Response amplitude operators for a freely floating cylinder obtained by the present  
 222 FEM and BEM also compared well.

223 Moreover, since the present study is based on a time domain formulation, nonlinear external  
 224 forces and moments acting over structures can be easily brought into the dynamics of the structure  
 225 interacting with waves. Nonlinear pressure boundary conditions have been implemented to show

226 how the algorithms can be used to evaluate wave energy converters based on oscillating water  
227 columns.

## 228 **Acknowledgements**

229 This study was partially supported by the Ministry for Science and Innovation of Spain in the  
230 AIDMAR project CTM2008-06565-C03-01. The authors are very thankful to Mr Rafael Watai for  
231 providing the numerical results from WAMIT showed in this work.

## 232 **References**

---

[1] Cai, X., Langtangen, H. P., Nielsen, B. F. & Tveito, A., A finite element method for fully nonlinear water waves. *J. Comput. Phys.* 1998; 143: 544–568.

[2] Oñate E. & García, J., A finite element method for fluid-structure interaction with surface waves using a finite calculus formulation, *Comp. Methods Appl. Mech. and Engrg.* 2001; 191: 635-660.

[3] Löhner, R., Yang, C. & Oñate, E., On the simulation of flows with violent free surface motion, *Comp. Methods Appl. Mech. Eng.* 2006; 195: 5597-5620.

[4] Löhner, R., Yang, C. & Oñate, E., On the simulation of flows with violent free surface motion and moving objects using unstructured meshes, *Comp. Methods Appl. Mech. Eng.* 2007; 53: 1315-1338.

[5] García, J., Valls A., & Oñate, E., ODDLS: A new unstructured mesh finite element method for the analysis of free surface flow problems, *Int. J. Numer. Meth. Fluids* 2008; 76 (9): 1297-1327.

[6] R. McCamy and R. Fuchs, Wave forces on piles: a diffraction theory, *Tech. Memo No. 69, U.S. Army Corps of Engrs.* 1954.